Journal of Pharmaceutical Sciences 110 (2021) 1444-1456

Contents lists available at ScienceDirect

Journal of Pharmaceutical Sciences

journal homepage: www.jpharmsci.org

Special Topic Cluster

Supercritical-CO_2 Foam Extrusion of Hydroxypropyl Methyl Cellulose Acetate Succinate/Itraconazole Amorphous Solid Dispersions: Processing-Structure-Property Relations

Shahab Kashani Rahimi [a], Kevin O'Donnell [b], Brian Haight [c], Augie Machado [c], Charlie Martin [c], Fan Meng [a], Tony Listro [d], Feng Zhang [a, *]

[a] College of Pharmacy, University of Texas at Austin, 2409 University Ave, Austin TX 78712
[b] DuPont Nutrition & Biosciences, Pharma Solutions, 1801 Larkin Center Drive, Midland MI 48674
[c] Leistritz Extrusion, 175 Mesiter Ave, Somerville NJ 08876
[d] Foster Delivery Sciences, 45 Ridge Road, Putnam CT 06260

ARTICLE INFO

Article history:
Received 8 June 2020
Revised 15 November 2020
Accepted 19 November 2020
Available online 5 December 2020

Keywords:
Extrusion
Bioavailability
Foaming
Amorphous Solid Dispersion(s) (ASD)
Milling
Compaction

ABSTRACT

This study investigates the effects of supercritical CO_2 as a foaming agent on structure and physical properties of hot melt extruded hydroxypropyl methylcellulose acetate succinate (HPMCAS)-itraconazole (ITZ) amorphous solid dispersions (ASDs) with the aim of improving the milling efficiency and tabletability of these ASDs. Two different grades of AFFINISOL™ HPMCAS, the standard grade (Std) and the High Productivity grade (HP) were used. The HP-grade has a lower molecular weight, melt viscosity and wider processing temperature range. Extrudates with different ITZ concentrations (0%, 20% and 40%) and CO_2 injection pressure of 100 and 200 bar were prepared.

The cellular microstructure of the foams showed that HP-grade HPMCAS had better affinity with the CO_2 resulting in better distribution of CO_2. The results of DSC and X-ray diffraction analysis revealed that the supercritical CO_2 did not affect the amorphous state of the API in the extrudates. Milling efficiency of the ASDs was significantly improved up to around 90% increase in the mass recovery. The tabletability of the milled extrudates showed a considerable increase in tablet tensile strength. In addition, foaming considerably improved the supersaturation of HP-grade ASD while showing minimal improvement in dissolution behavior of the Std-grade material.

© 2020 American Pharmacists Association®. Published by Elsevier Inc. All rights reserved.

Introduction

It is currently estimated that up to 70% of newly-discovered chemical entities in pharmaceutical pipelines and up to 40% of already marketed products belong to BCS class II or IV with a characteristic of being poorly water soluble compounds.[1,2] As a result of low solubility, the bioavailability of these active pharmaceutical ingredients (APIs) are significantly limited,[3] therefore, the efforts for development of novel processes for manufacturing of oral solid dosage forms with enhanced bioavailability of the API has been gaining traction. One of the most effective methods of increasing the apparent solubility and bioavailability of poorly soluble APIs is the amorphous solid dispersion (ASD) technology.[4] ASD is a blend of a polymer carrier in which the API is dispersed at the molecular level to form a metastable system (or solid solution). While the existence of the drug embedded in polymer matrix in amorphous and high energy state lowers the energy barrier for dissolution process (spring effect), the polymeric carrier stabilizes the supersaturated solution by preventing the precipitation and recrystallization of the drug (parachute effect) which ultimately, enhances the flux of the API across the intestinal mucus.[5,6]

Hot-melt extrusion (HME) is a well-known technique for preparation of amorphous solid dispersions due to a number of advantages in comparison to other traditional processes of ASDs such as high throughput, short process residence time, process design flexibility in terms of process variables and screw profile, ease of scale up and adaptability for in-line monitoring via process analytical technology (PAT) tools.[7] In addition, the absence of organic solvents during the process has significant cost, environmental and safety advantages. On other hand, there are some disadvantages associated with hot melt extrusion such as flowability

Conflict of Interest Statement: The authors have no conflicts of interest to declare and there is no financial interest to report. We certify that the submission is original work and is not under review at any other publication.

* Corresponding author.
E-mail address: feng.zhang@austin.utexas.edu (F. Zhang).

https://doi.org/10.1016/j.xphs.2020.11.038
0022-3549/© 2020 American Pharmacists Association®. Published by Elsevier Inc. All rights reserved.

issues of polymer carriers during the process,[8,9] high melting point of the API and potential thermal degradation of thermally labile or shear-sensitive APIs during the process.[10] Depending on the molecular state of the active ingredient in the matrix carrier, HME can be used to prepare amorphous solid dispersion, amorphous solid solution and crystalline sold dispersion.[11,12] With a proper knowledge of the design space for the HME process, which could be manifested in a diagram of energy input versus thermal history (which itself correlates with residence time distribution and temperature of the process), and selection of the process-tailored screw profile, both high extreme conditions that leads to degradation of polymer/API and low extreme conditions that leads to inhomogeneous polymer/API mixture could be avoided.[13]

The choice of the carrier polymer can drastically affect the performance of amorphous solid dispersions prepared by HME.[7,14] Typically, factors such as the glass transition temperature and melt viscosity of the polymer, specific polymer-API interactions through oppositely charged moieties or hydrogen bonding as well as the physico-chemical properties and stability of the polymer have significant implications on the process, performance and stability of the final ASD products.[15,16] Cowley *et al* [8] has provided a comprehensive review of the thermoplastic polymers suitable for HME. The most notable polymers used for HME process from industrial point of view are povidone, copovidone, hydroxypropyl methylcellulose acetate succinate (HPMCAS) and methacrylate-based polymer such as Eudragit® E100.[17]

One of the functional and efficient polymer carriers for HME processing of ASDs is HPMCAS. HPMCAS is a thermoplastic polymer with a set of unique characteristics such as high *Tg* (around 120 °C) that provides superior physical stability for the ASD, amphiphilic nature that enables it to interact with a wider range of hydrophobic APIs, and colloidal stability in solution at pH>5 due to its charged molecular state.[18] These unique characteristics make HPMCAS a suitable polymeric carrier for ASDs prepared using melt extrusion process. However, there are a number of challenges with HPMCAS based ASDs most notably its low milling efficiency and poor tableting behavior.[19,20]

Foam extrusion has traditionally been used in plastic industry for a wide range of automotive, insulation, energy absorbing and packaging applications.[21,22] Plastic foams can be categorized into three classes depending on the cell size as: macrocellular foams (cell size>100 μm), fine-celled foams (10 μm<cell size<100 μm) and microcellular foams (cell size<10 μm).[23] Thermoplastic foaming follows a two-step nucleation and growth mechanism. In nucleation phase, thermodynamic perturbations result in creation of new dispersed phase (bubble nuclei) which, if larger than the size of a critical nuclei, will spontaneously grow into larger domains. Upon releasing the pressure, the gas (foaming agent) evaporates leaving behind the cellular morphology.[24] Recently, foaming process has been successfully utilized in pharmaceutical HME process. Verreck *et al* [25,26] used both supercritical and pressurized CO_2 as a reversible foaming agent and plasticizer in hot melt extrusion of vinylpyrrolidone-vinyl acetate copolymers and ethylcellulose 20 cps polymer. Lower extrusion temperatures were achievable due to the plasticizing effect of CO_2 that reduced the melt viscosity of the polymers during the process. Ashour *et al* [27] studied the effects of pressurized CO_2 as a foaming agent on Klucel™ hydroxpropyl cellulose (HPC) / Ketoprofen extrudates. It was reported that foam extrusion considerably improved the API release rate and tabletability of the extrudates in addition to reduced tablet friability. Vo and coworkers[28] used sodium bicarbonate as a dual-functional foaming agent and microenvironment pH modulator in hot melt extrusion of HPMCAS/felodipine amorphous solid dispersion. They reported an 8-fold increase in supersaturation solubility of the API and considerably enhanced API dissolution in a two-step biorelevant medium.

In order to address the challenges of the HPMCAS amorphous solid dispersions, this study aims at application of supercritical (SC)-CO_2 for foam extrusion of AFFINISOL™ HPMCAS-itraconazole solid dispersions to improve the compaction and tabletability properties, milling efficiency and dissolution rate of milled HPMCAS/ITZ extrudates. A comparative study is conducted on the role of CO_2 injection pressure and the two grades of high and low molecular weight HPMCAS carrier. Itraconazole (ITZ) is a highly water insoluble drug (practical solubility of 1 ng/ml) with a partition coefficient of logP > 5 [25]. It is therefore, chosen as a model insoluble API for the foam extrusion process.

Materials and Methods

Materials and Extrusion Process

Standard (Std) and high productivity (HP) grade AFFINISOL™ HPMCAS was kindly supplied by DuPont Nutrition and Biosciences (Midland, MI). The Characteristics of both grades are detailed in Table 1. Itraconazole was obtained from Shenzhen Nexconn Pharmaceutics (Shenzhen, China). Formulations are based on 0, 20 and 40 wt% of itraconazole and 1% of talc as a foam nucleating agent. The samples are coded as “X%-Y” where X denotes the API content and Y corresponds to the grade of the matrix polymer. “Control” sample refers to the unfoamed extrudates.

The extrusion process was conducted on a Leistritz ZSE 18mm HP twin screw extruder with 40:1 L/D ratio with the screw and barrel temperature profiles as shown in Fig. 1. Note that for Std-grade samples only 40% ITZ compositions were extruded. The extruder consisted of 8-barrel zones with a preset temperature profile as shown in Fig. 1 which was dependent on the grade of the HPMCAS.

It is important to note that the lower die temperature was used in HP-grade in order to prevent the melt collapse upon foaming due to the lower viscosity of this grade. The extrduate should possess enough melt elasticity and viscosity to withstand the internal foaming pressure to prevent the collapse of the cellular structure. Prior to the injection point of the SC-CO_2 (zone 3), a combination of neutral kneading elements with 90º stagger angle and a reverse GFA element was used to create a dynamic melt seal zone to prevent the backflow of CO_2 towards the feed. The SC-CO_2 flow was regulated using a Waters Thar model P high pressure pump at two different injection pressures of SC-CO_2 at 100 bars (denoted as “lowP”) and 200 bars (denoted as “highP”) were used. Selection of the CO2 pressure was experimentally obtained. Pressure of 100 bars was the minimum pressure that allowed for development of foamed samples. It was then decided to increase to pressure to 200 bars so that a cellular foamed samples could be achieved while the effect of different injection pressure could be studied. Further increase in the pressure resulted in significant increase in the torque value during the extrusion. Therefore, we settled with 100 and 200 bars as our low and high pressure settings. The 40% HP-grade

Table 1
Specifications of HP- and Std-Grade AFFINISOL HPMCAS.

Property	AFFINISOL™ HPMCAS 912	AFFINISOL™ HP HPMCAS 912
Methoxy (wt%)	21-25	21-25
Hydroxypropyl (wt%)	5-9	5-9
Acetate (wt%)	7-11	7-11
Succinate (wt%)	10-14	10-14
Viscosity (mPa.s)	3	2
Molecular weight (kDa)	100-200	10-90
pH dissolution	6	6

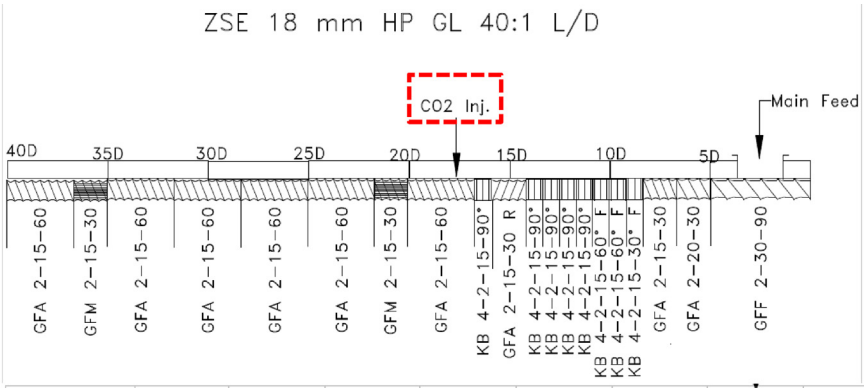

Zone 8	Zone 7	Zone 6	Zone 5	Zone 4	Zone 3	Zone 2	Zone 1	Grade/zone
133 °C	133 °C	133 °C	150 °C	150 °C	160 °C	160 °C	77 °C	HP
144 °C	133 °C	133 °C	150 °C	150 °C	160 °C	160 °C	90 °C	Std

Fig. 1. Screw and temperature profile of the foam extrusion process. GFF X-XX-XX and GFA X-XX-XX denote a non-self-wiping and self-wiping co-rotating conveying elements with number of flights, pitch length (mm) and element length (mm) respectively. KB X-X-XX-XX denotes a kneading element with disc thickness (mm), number of flights, element length (mm) and staggering angle (°). GFM X-XX-XX denotes a mixing element with number of flights, pitch length (mm) and element length (mm).

sample injected with high pressure setting of SC-CO_2 was omitted as the viscosity of this sample was not sufficient to support the cellular structure during the foam development phase.

The screw speed was optimized via a number of preliminary experiments with each HPMCAS grade and set to 50 and 100 rpm for HP-grade and Std-grade respectively. The lower screw speed for HP-grade material prevented excessive reduction of viscosity and subsequent collapse of the foam strand. Powder blend was fed at the rate 1 kg/hr. The physical mixture of the polymer and API was prepared by physically blending in a Maxiblend V-blender (GlobePharma, New Brunswick, NJ) at 25 rpm for 10 minutes.

Analysis of Milling Efficiency and Particle Size Distribution

Foam and control samples were milled using a model F1A Fitzpatrick Fitzmill (Westwood, MA) equipped with a 0.5 mm mesh screen running at 3500 rpm. About 80 g of the sample were fed at a rate of 20 g/min to the milling hopper (4 minutes) followed by a 2-minute additional milling time. The amount of material retained inside the mill (within the specified milling time) as well as the instrument torque were used for assessment of the milling efficiency.

The particle size distribution of the milled extrudates was obtained on a Tyler model RX-24 sieve shaker (Mentor, OH) with size fractions of 63 μm, 125 μm, 250 μm and 425 μm. For this purpose, about 50 g of the milled sample was placed on the stacked sieves and vibrated for 6 minutes. The mass of the samples collected on each sieve was used to construct the particle size distribution.

Analysis of Morphology by Scanning Electron Microscopy

The morphology and structure of the foams were studied by FEI Quanta® 650 (Hillsboro, OR) Scanning Electron Microscope operating at 10 kV. The samples were consolidated on aluminum stubs using double sided carbon tapes and a conductive carbon paste and sputter coated with silver using an ESM 550 sputter coater prior to analysis.

Differential Scanning Calorimetry and X-Ray Diffraction

Thermal analysis of the samples was conducted using a TA Instruments Q20® DSC (New Castle, DE) via a heat-cool-heat program with 20 °C/min heating/cooling rate under dry nitrogen atmosphere with a flow rate of 50 mL/min. About 4-7 mg of the powder sample was placed in hermetic aluminum pans (with a small hole punched in the lid) and the experiment was conducted in triplicates for each sample. The data was analyzed using Universal Analysis software.

The crystallinity of the amorphous solid dispersions was assessed using a Rigaku Miniflex 600 X-ray diffractometer (Tokyo, Japan). Analysis was performed with 2 °/min scan rate and 0.02 ° step in the 2θ range of 4-50 °.

Melt Rheological Properties

The rheological properties of the ASDs were studied on a TA Instruments ARES 2000 (New Castle, DE) shear rheometer using a parallel plate geometry with a gap setting of 1 mm and temperature of 160 °C under dry nitrogen atmosphere. Dynamic frequency sweep tests were conducted on control (unfoamed) samples at a 5% strain rate and angular frequency range of 0.1-200 rad/s. A strain sweep test was performed prior to the test to find the linear viscoelastic region. A thermal soak time of 90 s was applied prior to frequency sweep analysis to eliminate the residual stress in the samples. Relaxation was monitored by a time sweep test to ensure constant viscoelastic properties over the whole period of frequency sweep tests.

Mechanical Properties

The mechanical properties of the extrudates were studied using a TA.XT*Plus* texture analyzer (Texture Technologies, Hamilton, MA). The extrudate strands were carefully cut into cylindrical segments with a razor blade and then subjected to diametral compression force using a TA-10 plastic flat head tip with a diameter of 12.6 mm. The geometrical features of the samples were carefully adjusted to ensure its compliance of the requirement of ASTM D3967-16 regarding thickness-to-diameter ratio of 0.2-0.75. The samples were compressed with a head speed of 0.8 mm/s up to 40% compressive strain. A return trigger force of 0.1 N was programmed so that the blade would stop the compressive force and return to the original position if the samples failed prior to reaching the 40% strain. At least 5 replicates for each sample were tested and the force-displacement data were converted to stress-strain

curve. The data was obtained using Exponent software (version 7.0.1.0). The probe height, force and frame deflection were calibrated using the Exponent software prior to testing of the samples. The work of fracture was obtained by integrating the stress-strain curve using Origin Pro® software.

Specific Surface Area and Porosity

Specific surface area of the milled extrudates in the size fraction of 250- 425 μm was studied by the Brunauer-Emmett-Teller (BET) method using a Monosorb™ Quantachrome (Quantachrome Instruments, Boynton, FL) gas adsorption analyzer. All the powder samples (200-500 mg sample size) were degassed overnight prior to the measurement by purging with helium at 50 °C on the Thermoflow Degasser (Quantachrome Instruments). A mixture of nitrogen and helium (30/70 mol%) was used as the adsorbate. For each sample, 5 adsorption-desorption cycles were performed. The average and standard deviation values are reported. Particle porosity was measured by mercury intrusion porosimetry on a Micromeritics AutoPore IV 9500 Series instrument (Atlanta, GA) using particle size fraction of 250-425 μm. About 1.6 g of powder was weighted and loaded into the penetrometer. The penetrometer was degassed for 5 minutes with evacuation pressure of 50 μmHg in a vacuum and then filled with mercury at 1.92 psia. The equilibration time was 45 seconds.

Tabletability and Compaction Properties

Compaction behavior and tablet mechanical properties were assessed using a benchtop Carver lab press (Wabash, IN) operated at compression pressures of 2000-5000 psi followed by measurement of tablet hardness. A blend of the milled extrudate (taken from the 250-425 μm size fraction) with microcrystalline cellulose (MCC) with a weight ratio of 80:20 was premixed using the V-blender (25 rpm, 10 minutes) and used for compaction tests. This blend ratio was found to be compressible enough to showcase the differences in compressibility/compaction property of the extrudate while not too compatible to negate the inherent compactibility of the extrudate. All experiments were performed in triplicates. The tablet tensile strength was calculated using the hardness values based on the Equation (1) as follows [29]:

$$\sigma = \frac{2F}{\pi DH} \quad (1)$$

where the F is the breaking force of the tablet (obtained from hardness value in *kp*), D is the tablet diameter and H is the tablet thickness.

Challenging 40% drug load formulations were selected for the tabletability study so that the effect of the foaming process and its improvement on compaction of the powder could be better observed and studied. Samples with lower drug load would propose better intrinsic compressibility/compactability.

Non-Sink Dissolution Testing

In-vitro drug release experiments were performed on the milled extrudates (250-425 μm size fraction) to examine the effect of the foaming process and the HPMCAS grade on the release rate of the ITZ from the extrudates. A Varian VK7000 (Cary, NC) dissolution apparatus operating at the paddle speed of 75 rpm at 37 ± 0.5 °C using the amount of the milled powder that correlated to 130 μg/mL nominal concertation of API was used. The dissolution medium was a pH 6.8 phosphate buffer. At predetermined time intervals, 2 mL aliquots of the medium were taken and centrifuged at 12000 rcf on a Microfuge 18® (Beckman Coulter, Brea, CA). The supernatant was removed and diluted with acetonitrile by a factor of 2 and then analyzed via a reversed phase HPLC method.

An isocratic method was developed to measure the concentration of ITZ in the samples. A Waters® HPLC system (Waters corporation, Milford, MA) consisting of a Waters® 2996 PDA detector, a 717 Plus autosampler, and a Waters® 515 pump. A 55:45 (v/v) water/acetonitrile mixture containing 0.05% trifluoroacetic acid (TFA) was used as a mobile phase. Samples were injected at the volume of 10 μL through an Agilent Poroshell™ 120 C18 column (4.6 mm × 50 mm, 2.7 μm) with a flow rate of 1 ml/min and analyzed at 262 nm. The retention time of ITZ was 3.5 minutes.

Results and Discussion

Extrusion Process, Morphology and Rheological Properties

In this study, the extrusion temperature, HPMCAS grade, screw speed and polymer-API ratio were found to significantly affect the foam extrusion process. In the case of the HP-grade material, use of higher screw speed (100 rpm) significantly decreased the viscosity (at the temperature profile used) due to shear thinning which prevented successful foaming of the melt strands. This was even more problematic as the API content increased. Temperature of the process was selected as the minimum possible temperature to achieve ASDs. In addition, for both HP- and Std-grade HPMCAS, it was observed that the foaming could not be achieved in the absence of talc as a nucleating agent. This was primarily due to extremely low cell density and formation of excessively large bubbles without talc. In addition, the SC-CO_2 did not impart any plasticizing effect on the polymer melt as the motor load slightly increased with injection of the CO_2. For example, in the case of the 40% Std-grade sample, application of lowP (100 bar) and highP (200 bar) injection pressures increased the 50% load in the control sample to 51 and 53%, respectively. This is similar to the observations of Almutairi et al [30] where injection of pressurized CO_2 did not show any plasticizing effect on the AquaSolve™ HPMCAS extrusion. In addition, a potential local drop of temperature at the injection site and thereby a short transient increase in viscosity may contribute to the increase in torque.

The cellular morphology of the foamed samples is shown in Fig. 2. As evident in the Fig. 2a, in the samples containing no API, the cellular structure in the HP-grade lowP (100 bar) foam ranges within 20-200 μm. As the injection pressure increases to 200 bars (highP) the cell wall thickness decreases, and cell size increases to 50-300 μm. In contrast, the Std-grade foams show minimal dependency of cellular structure on the injection pressure and the cells is within 150-400 μm. Based on the cell size, the HPMCAS foams therefore belong to macrocellular foam category. It is also apparent that the distribution of the voids is more uniform in the case of HP-grade HPMCAS which is associated with higher cell density. There are a number of reasons proposed for the observed differences in the cell structure and size. First of all, the HP-grade polymer has a lower molecular weight and melt viscosity and elasticity (as will be discussed in the rheology section) that reduces extrudates' mechanical strength needed to support the cellular structure. In addition, due to the higher number of chain ends and larger free volume because of the lower molecular weight of HP-grade HPMCAS, the solubility of the CO_2 is higher in the polymer.[31,32] This leads to more uniform dispersion of CO_2 within the HP-grade matrix resulting in larger cell nuclei density. As a result, larger number of bubbles per volume (but smaller in size) form in HP-grade HPMCAS.

To further elaborate on this, from the chemical interaction perspective, the carbon on the CO_2 (electrophilic) undergoes acid-

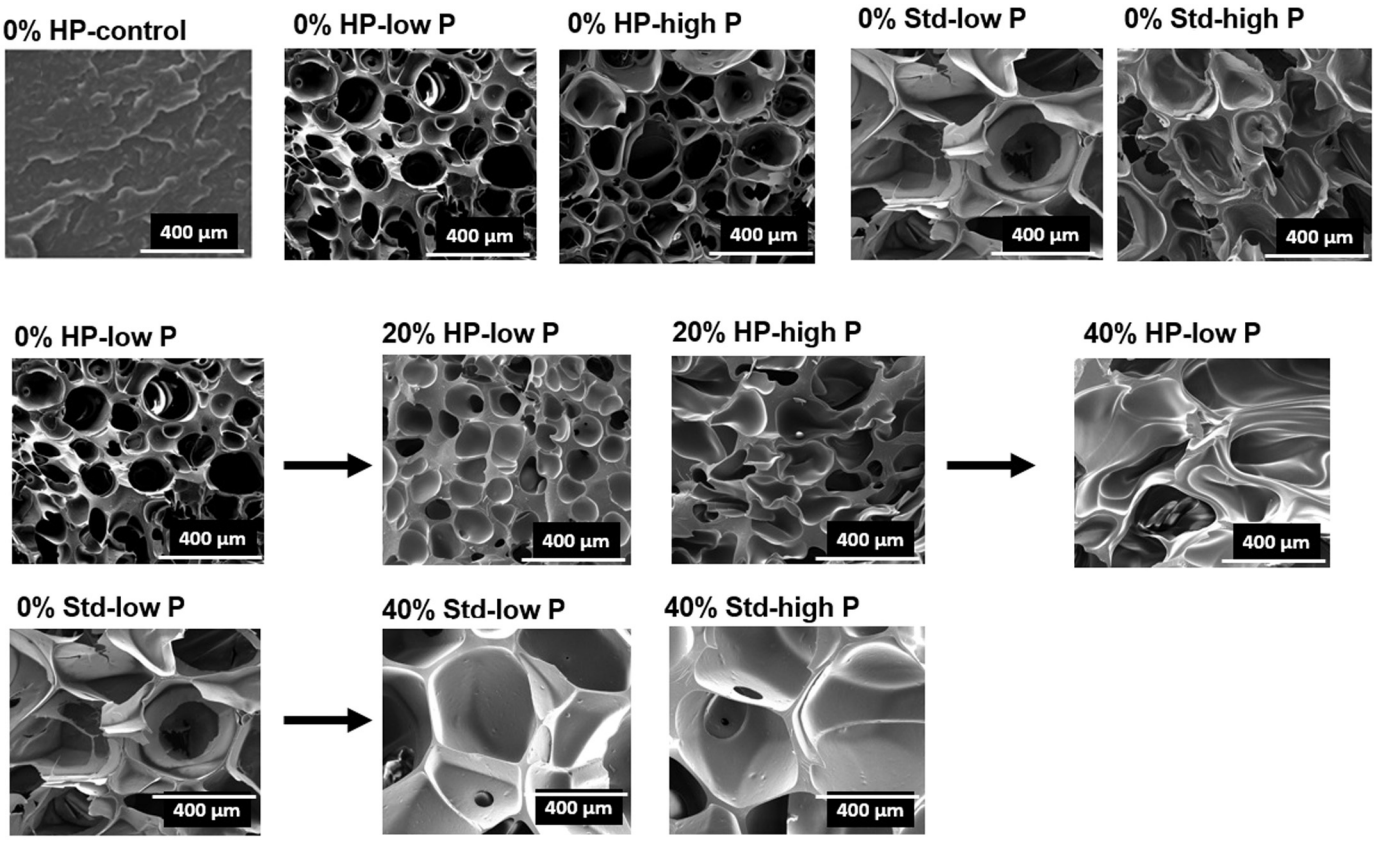

Fig. 2. SEM images of (a) control and foamed 0%API extrudates showing the variation of cell structure with HPMCAS grade and CO_2 pressure, (b)variation of cellular morphology of HP-grade extrudates with change in API concentration and (c) variation of cellular morphology of Std-grade extrudates at 0 and 40% API content.

based type interactions with the electron rich oxygen on the carbonyl group. As the molecular weight of the HPMCAS decreases, there will be higher density of carbonyl groups (because of higher chains ends) due to the presence of aldehyde at the reducing end of the glucose units. This is due to conversion of hemiacetal moieties (masked reducing end) to their open forms and thus, formation of more carbonyl groups. From the physical perspective, based on lattice model, higher chains ends result in increase in the free volume (microvoids) available for penetrant (CO_2 molecules) resulting in increased interactions/solubility.[31,32]

The effect of increasing the API concertation in the formulation is also evident on the microstructure of the cellular foam. It is seen in Fig. 2b that increasing the API concentration from 0 to 20 wt% in the case of HP-grade matrix, for the lowP setting, the structure resembles that of the 0% API, however, the highP setting significantly distorts the round shape of the cells and further increasing the API content to 40%, the cells become larger and become completely geometrically irregular. This shift in microstructure is attributed to the reduction of the melt viscosity of the formulation resulting in lower strength and cell wall stability under the internal pressure of bubble growth process. Similarly, in the case of Std-grade sample (Fig. 2c), increasing the API content to 40% results in formation of larger bubbles; however, unlike the HP-grade sample, the truncated octahedron shape of the cells are retained which is due to the higher melt strength of the Std-grade that withstands the bubble growth pressure even at higher API content.

The rheological properties of the thermoplastic materials is a key variable in defining the foamability of the melt matrix. The rheological properties affects the distribution and flow of the foaming agent within the polymer as well as the nucleation and growth mechanisms of the bubble as the material flows out of the die. For example, a number of previous studies[33-35] have shown that the extensional viscosity of the polymer melt is an essential property for maintaining cellular morphology as the polymer melt in the bubble growth front is subjected to biaxial stretching. It has also been shown that sufficient extensional viscosity and melt strength is critical in achieving minimum melt rupture and collapse of the cellular “frames” during the growth stage.

In the current study, the effect of API content and HPMCAS grade on rheological properties of the formulations are discussed in terms of the variation viscosity and viscoelastic properties of the formulations in melt state. The variation of complex viscosity of the control samples as a function of the HPMCAS grade and API content is shown in Fig. 3a. It is evident in this graph that the Std-grade HPMCAS has higher melt viscosity at all API compositions. With an increase in the API content, the viscosity reduces in both Std- and HP-grade HPMCAS. The difference in the viscosity of the formulations further increases with increasing the API content. As seen in the samples containing 40% API, the difference in complex viscosity values are larger compared to that of neat polymers. The shear thinning index of the formulations are shown in Fig. 3a. As the API content is increased, the shear thinning index decreases which indicates that higher API content compositions have viscosities that are less dependent on shear rate. This is primarily due to the fact that the API acts as plasticizer increasing the intramolecular free volume of the polymer, resulting in less chain entanglements and flow restriction in the shear field. The Std-grade sample has higher shear thinning property which shows that the rheological properties of the HP-grade based formulations are less shear-dependent. Rather than for the design of process, rheological data was to correlate the flow characteristics of the polymer-API blend to the foaming behavior and cellular microstructure. The

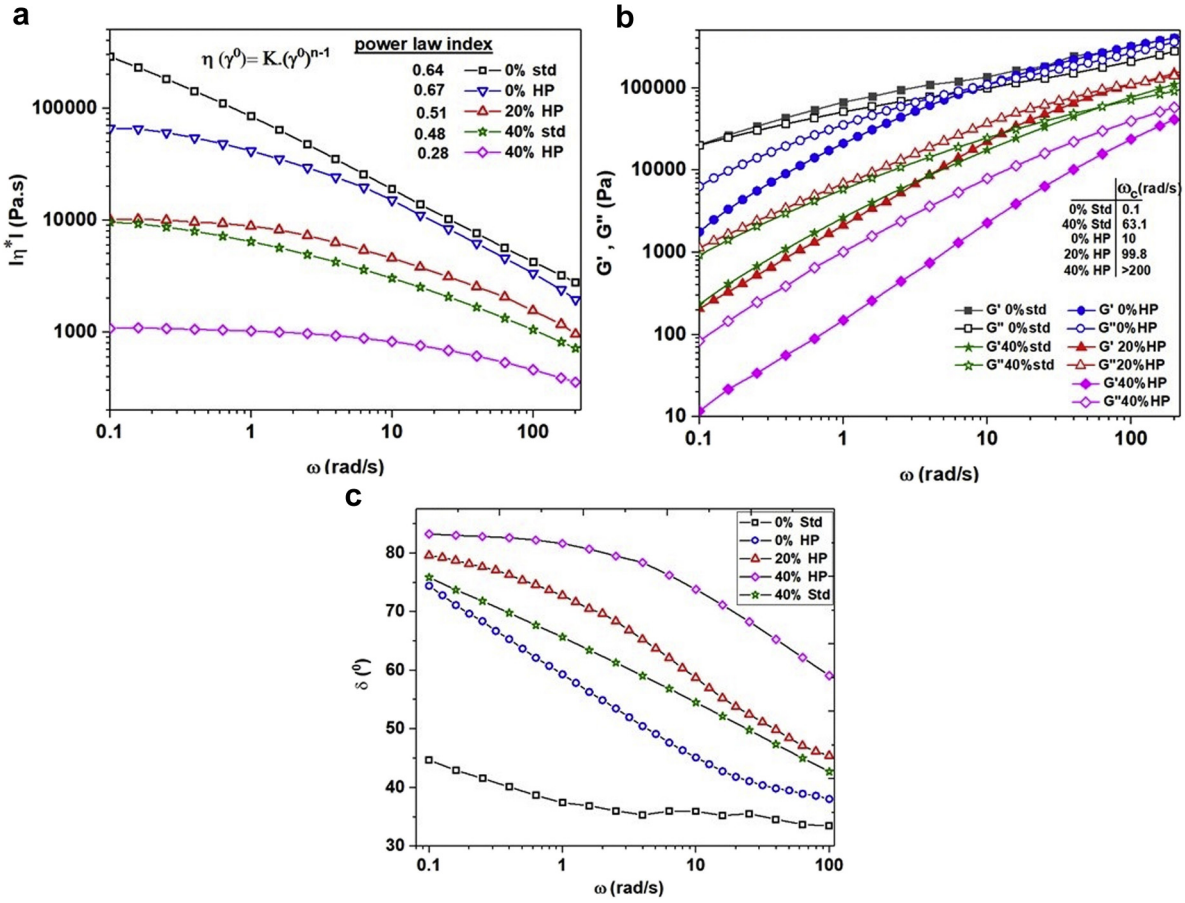

Fig. 3. (a) Complex viscosity, (b) elastic and loss modulus and (c) phase angle of extruded HPMCAS with 0, 20 and 40% API at 160 ºC.

extrusion conditions were experimentally determined due to the complex nature of this pressurized system.

One of the important rheological characteristics of the polymer melts that affects the foaming process is their extensional viscosity and an associated phenomenon known as strain hardening. Strain hardening has been shown to be the prominent factor in foamability of thermoplastics which originates in elastic contributions such as those imparted with long chain branching[36,37] or specific molecular characteristics and structure formation in extension.[38] The strain hardening coefficient is dependent on the transient extensional viscosity ($\eta_E^+(t, \varepsilon_0)$) and transient extensional viscosity in the linear viscoelastic region ($\eta_{E0}^+(t)$). Although the extensional viscosity of the pure HPMCAS grades and the ASD melts were not directly measured in the current study, however, the correlation of shear viscosity with extensional viscosity via Trouton ratio[39] ($(\eta_{E0}^+(t)=3\eta_0$ for Newtonian liquids and $\eta_{E0}^+(t)>3\eta_0$ for viscoelastic melts) shows that the extensional viscosity of Std-grade HPMCAS is higher than that of the HP grade especially considering typical foaming Hencky strain rates (1-10 s^{-1})[40] where elastic contribution becomes significant in the evolution of strain dependent extensional viscosities. A similar trend is expected with regard to samples with lower API content. Consequently, it can be inferred that the Std-grade HPMCAS and those with lower API content, exhibit enhanced strain hardening during the foaming process resulting in enhanced resistance towards melt rupture and structure collapse under process induced stresses. This is primarily due to higher molecular weight and chain entanglements in the of Std-grade melt that enhances the elasticity of the Std-grade HPMCAS during the foaming process.

The variation of the elastic and loss moduli of the HPMCAS-itraconazole ASDs with the two polymer grades and different API content is shown in Fig. 3b. It is clearly evident that increasing the API content significantly reduces the elastic modulus (G') of the melt. At similar API content, the Std-grade HPMCAS has higher elasticity compared to the HP-grade. The intersection of the G' and G" represents the relaxation time of the melt under experimental condition. It is observed that relaxation times ($\tau_R \sim 1/\omega_c$) for the Std- and HP-grade formulations (without API) are 10 and 0.1s respectively. The relaxation time of the HP-grade with 20% and 40% API decreases to 0.008s and a value smaller than 0.005s while for the Std-grade ASD with 40% API it decreases to 0.016s. These variations clearly show that the Std-grade formulations undergo significantly less viscous deformations under the applied internal foaming pressure during solidification after extrusion. It is also evident that increasing the API content within the melt, the relaxation time significantly reduces denoting a significant decrease in melt strength necessary to withstand the biaxial stresses of bubble growth phase. The effects of formulation on melt elasticity can also be elaborated via the variation of the phase angle of the dynamic stress response as shown in Fig. 3c. It is seen that at low frequency (terminal) region (<1 rad/s), the Std-grade sample has considerably lower phase angle denoting the high melt elasticity of this material which is a crucial property in prevention of cellular structure collapse during growth and melt solidification. In addition, increasing the API concentration significantly increase the phase angle towards 90º which corresponds to viscous deformation of the melt that is detrimental to structural integrity of the cellular structure during foaming process.

Thermal properties and crystallinity

The thermal properties and crystallinity of the amorphous solid dispersions were studied using DSC and XRD techniques to understand the impact of the foaming on crystalline nature of the ITZ in ASDs. The results of DSC experiments are shown in Fig. 4a-4c. It is seen in Fig. 4a that pure ITZ shows a sharp melting peak at 169 °C. In the physical mixture of HPMCAS (HP)/ITZ, two melting endotherms appear, the major peak at 168 °C and a smaller endotherm at 146 °C which correlated to a fraction of the API strongly interacting with the HPMCAS polymer. The two HPMCAS grades show a glass transition temperature at around 121 °C and 118 °C (for Std- and HP-grade respectively). As shown in Fig. 4b, the endothermic peak corresponding to the melting of crystalline ITZ completely disappears indicative of amorphous state of the ITZ drug in the extrudates in all ASD formulations. The incorporation of SC-CO_2 during the process and foaming of the extrudate does not affect the amorphous state of the API. The glass transition (first heat run) of the control and foam samples are shown in the Fig. 4b.

The endotherm around the Tg of the samples in both lowP and highP foams is attributed to the residual CO_2 and moisture in the foam samples that is completely removed in the first heating run as evidenced by the disappearance of the endotherm in the second heat runs as shown in Fig. 4c. In the second heat runs (Fig. 4c), there is only a single glass transition in all ASD samples indicative of complete miscibility of API and the HPMCAS matrix (since samples are heated above the melting point of drug).

The X-ray diffractograms of individual components, physical mixture, and foamed extrudates are shown in Fig. S1 (Supplemental Data). The absence of sharp characteristic peak of crystalline ITZ and the presence of a halo in X-ray diffractograms of extrudate samples indicated that ITZ is in amorphous state. It is also evident from the XRD analysis that the foaming process has no negative impact on the amorphization of ITZ within the polymer matrix. This is consistent with DSC results.

Milling Efficiency, Mechanical and Compaction Properties

The effect of the foaming process on the milling efficiency of the HPMCAS/ITZ extrudates was studied by measuring the extrudate mass recovery after milling. The milling yield shows the amount of the material that passes through the 0.5 mm opening during

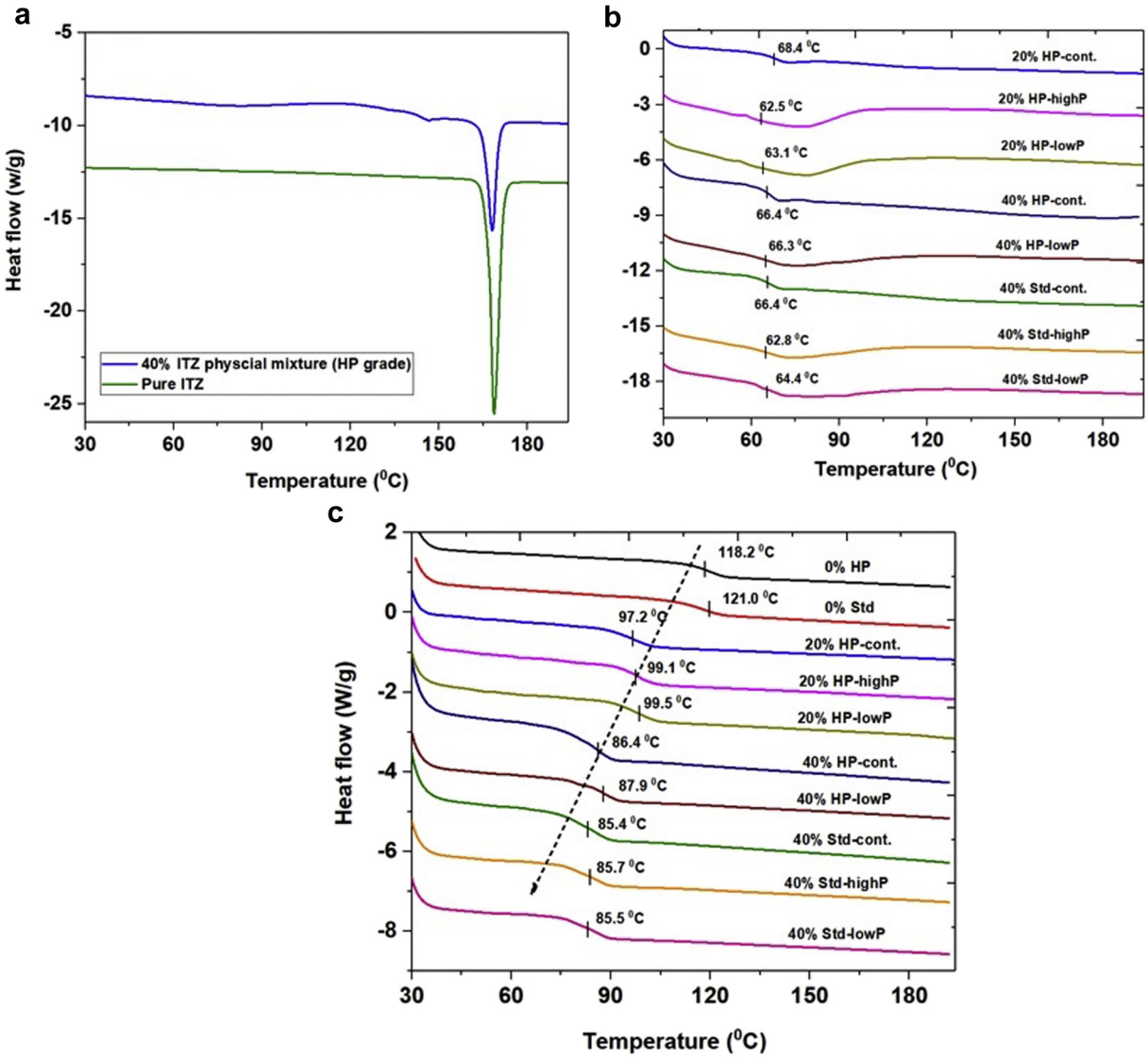

Fig. 4. DSC thermograms of (a) pure drug and physical mixture, (b) first heat run of extrudates and (c) second heat run of extrudates with the heat rate of 20 °C/min.

milling over the mass fed into the mill. The higher mass recovery indicates that the extrudates is easier to mill and the particle size of the milled product within the specified milling period is small enough to pass the 0.5 mm screen. Plots of the milling efficiency (yield) for the Std- and HP-grade HPMCAS based ASDs with various API content (0-40%) is shown in Fig. 5a and b. For the Std-grade HPMCAS (in absence of API), foaming process at lowP and highP can significantly increase the yield from around 58% up to 88% and 92%, respectively. In the case of the HP-grade sample, the yield of the milling process increases from around 82% to more than 95% at both pressure settings. For the 20% HP-grade sample, the yield increases from an average of 85% in the control sample to values of above 95% for both lowP and highP extrudates. Additionally, for the 40% API both Std-grade and HP-grade extrudates are easier to mill (as indicated by higher milling efficiency of control samples) where the milling efficiency increases to above 90%. In addition to the yield of the milling process, torque of the Fitzmill indicated a considerable decrease as a result of the foaming process. For example, the torque reading reduced from 1.05 amps for control Std-grade to 0.75 and 0.73 amps in the case of lowP and highP foamed samples. This lower energy input prevents excessive increase of the extrudate temperature during the milling process and avoids mesh blockage by softened polymer.

It is evident that foaming process is an effective strategy to enhance the milling behavior of the hard-to-mill extrudates such as those based on HPMCAS. The cellular structure and internal voids of the foamed samples provides a significant number of stress-concertation "weak" points that results in brittle fracture of the foamed samples due to the impact of the rotating blade. In addition, as shown in Fig. 5c, during the milling process of the control Std-grade HPMCAS (and to a lesser extent in the case of control HP-grade sample), there was a build-up of material inside the mill (due to resistance of the sample against particle attrition) which resulted in significant increase of temperature and consequent softening of the polymer that smeared on and blocked the screen, preventing further passage of particles. However, in the case of foamed samples, due to rapid fracture of the extrudate and reduction of particle size, all the material passed through the 0.5 mm screen without any blockage or build-up. Similar observation was also reported in the work of Ashoura et al [27] on HPC-ketoprofen control versus foamed extrudates.

It should also be noted that the HP-grade HPMCAS is a suitable alternative for the Std-grade from the milling perspective. Regardless of the foaming process, the HP-grade samples show significantly higher milling yield (even in the control samples) without any material build-up and screen blockage during the milling process, highlighting the advantage of using HP-grade HPMCAS for preparation of HPMCAS-based ASDs using melt extrusion.

Another approach of evaluating the milling process is to investigate the particle size distribution of the milled product. The particle size of the milled extrudates was studied by sieve analysis. The d_{50} values of the obtained milled particles are shown in Fig. 6a. As can be seen, compared to the Std-grade, the HP-grade has considerably lower average particle size in all similar processing conditions both in control and foam samples. This shows that the

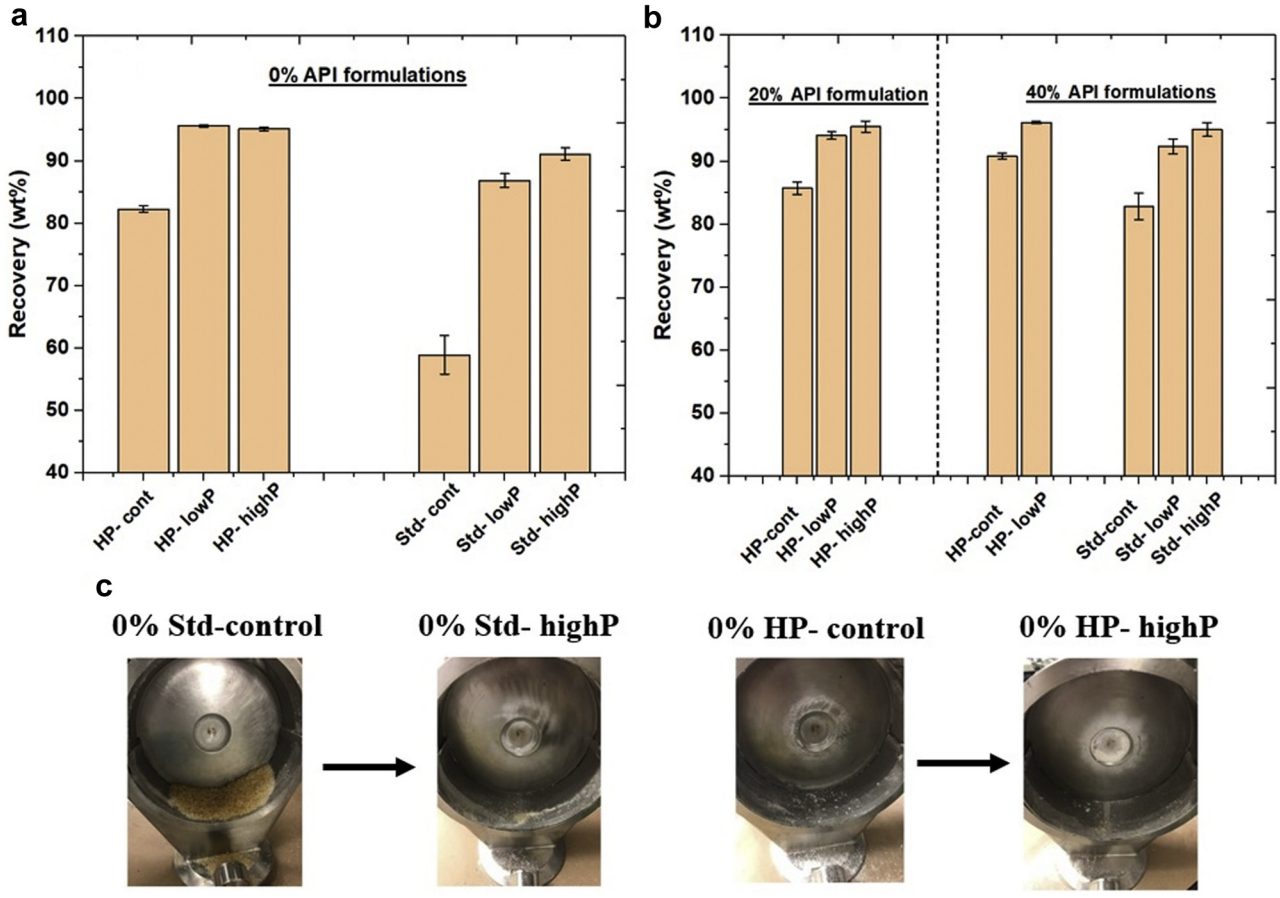

Fig. 5. Milling efficiency of control and foamed extrudates with (a) 0% API, (b) 20 and 40% API and (c) build-up of Std- and HP-grade grade HPMCAS extrudates during the milling process.

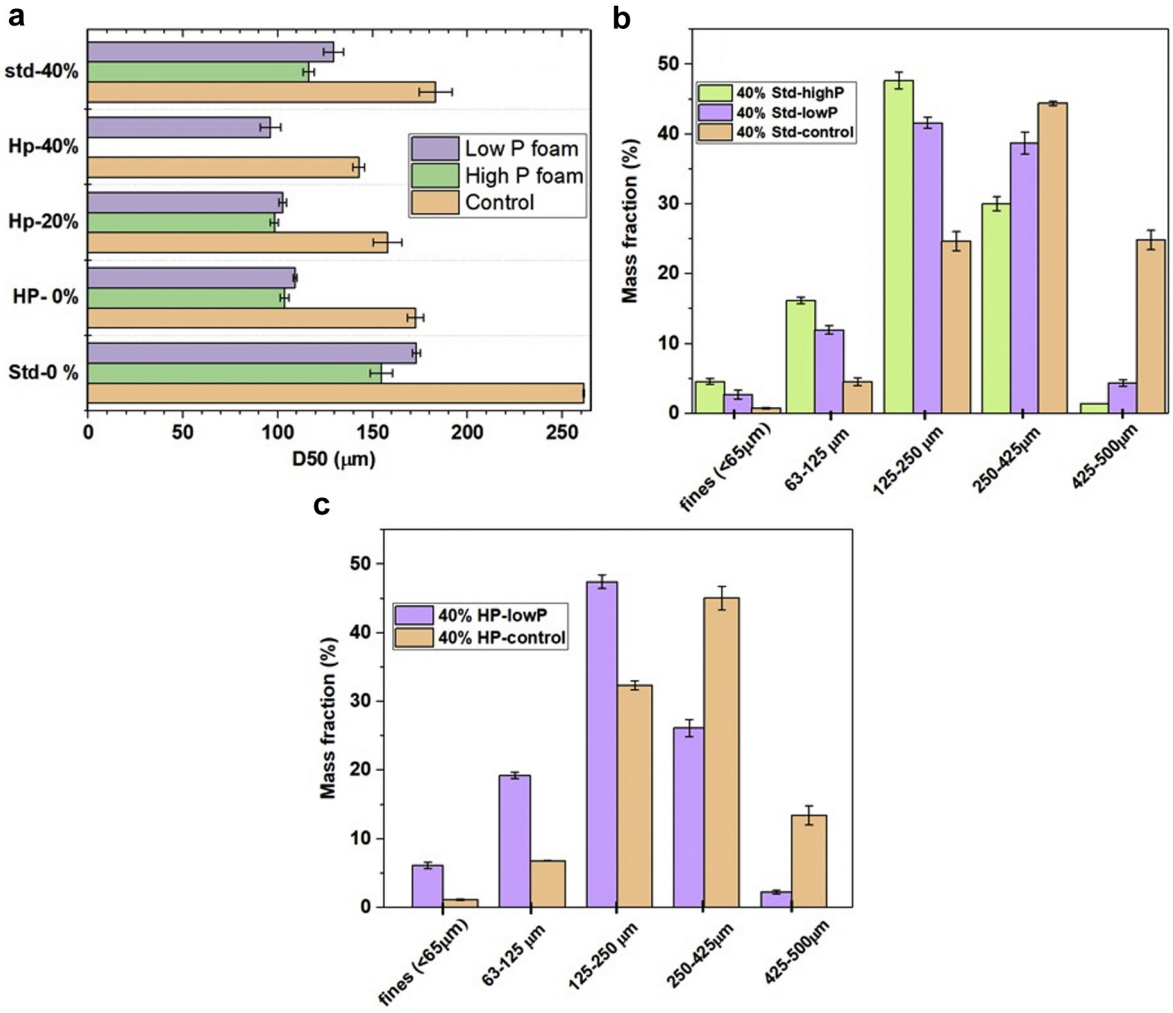

Fig. 6. (a) Variation of d_{50} vs HPMCAS grade and foaming pressure, particle size distribution of (b) 40% Std-grade and (c) 40% HP-grade of control and foam samples.

HP-grade is a more efficient alternative to Std-grade in terms of achieving smaller particles after milling.

In addition, a representative size distribution plot for the 40% control and foamed extrudates are shown in Fig. 6b and c. In the case of 40% HP-grade sample, upon foaming, the fractions of 250-425 μm and that of above 425 μm decreased from 45% and 14% to 25% and 3% respectively while the fractions of 125-250 μm and 63-125 μm increased from 33% and 7% to 47% and 19 % respectively showing the considerable decrease in the particle size of the foamed samples during milling process.

Similarly, in the case of 40% Std-grade samples, foaming with highP condition increased the fraction of 125-250 μm from around 25% to above 40% and decreased the largest particle fractions (>425 μm) from 25% to below 5% indicative of high efficiency of foaming process to reduce the particle size of the milled extrudates to the fractions suitable for tableting. The average D50 value for 40% Std-grade sample decreases from 183±8 μm to 129±5 μm and 116±3 μm in highP and lowP foams. For the HP-grade sample, the lowP foam has an average d50 value of 96±5 μm as opposed to 143±3 μm in the control sample.

In order to better understand the effect of the HPMCAS grade and the foaming process on milling performance of ASDs, the mechanical properties of the extrudates were studied by diametral compression test using a texture analyzer. In this experiment, the chopped extrudates (from pellet cutter) were trimmed into cylindrical specimens and tested diametrically under compressive force and the force- displacement data were then converted to stress-strain (SS) plots as shown in representative plots of Fig. 7. The fracture strength is the ultimate point on the stress curve where the sample failed under compressive force. The work of fracture is the energy needed in order to bring the material to the ultimate stress point by integrating the stress-strain curve ($E = \int_0^{\varepsilon_B} \sigma d\varepsilon$). The values of ultimate fracture strength and work (energy) of fracture are given in Table 2 (The stress-strain plots for control and foam samples containing 0% API are provided in Fig. S2 in Supplemental Data).

First of all, it is evident from the SS plots that the Std-grade HPMCAS has superior intrinsic mechanical properties compared to the HP-grade due to its higher molecular weight. For all of the Std- and HP-grade control samples (any API concentration) the fracture stress and the work of fracture is considerably higher in the case of the Std-grade while with addition and increase in the API concentration, both the strength and work of fracture decrease. In addition, the foaming significantly decreases the fracture strength and the energy required to fracture the samples. The work of fracture shows two orders of magnitude reduction with foaming. This is primarily due to the presence of voids and pores within the material structure acting as structural "defects" when the material is subjected to external stress. Also, the cell walls of the cellular structure are stress-concentration points under the compressive load. Another important consideration of the SS plots of the foam

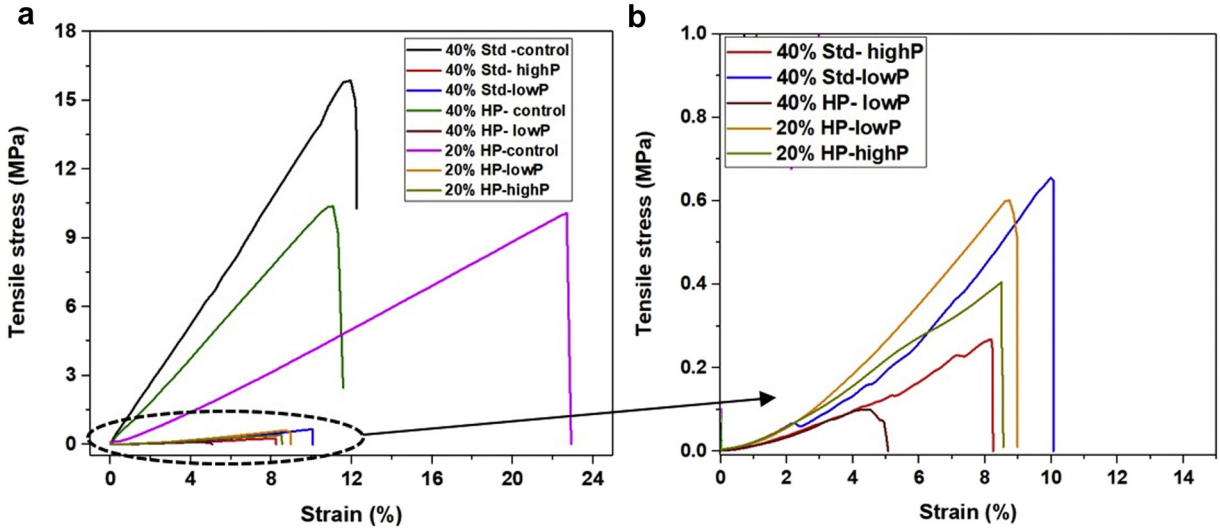

Fig. 7. Stress-strain plots of (a) control and (b) foamed extrudates with 20 and 40% API (zoomed-in area of (a)).

samples is the reduction of strain-to-break. This shows that foaming not only decreases the strength of the sample, but also decreases the toughness of the extrudates, rendering the material more brittle with less deformation prior to fracture. This is an important characteristic as the foamed extrudates would fragment instantly during the milling process without undergoing energy-absorbing plastic deformation.

The variation of porosity and BET specific surface area of the control and foamed samples are also shown in Table 2. Clearly, the porosity of the samples significantly increases as a result of the foaming process. The porosity of the foams decreases as the API content is increased which is attributed to the reduction of the viscosity of the samples with higher API content (as discussed before) and subsequent compromise of the cellular structure due to rupture and collapse of the capillary cell walls. Increasing the SC-CO_2 injection pressure slightly increases the overall porosity. In addition, for the samples without API, it is evident that the porosity of the HP-grade at both lowP and highP foams are higher than those of the Std-grade. This trend is however, opposite for the 40% API samples due to significant reduction of the viscosity of the 40% HP-grade sample. Similarly, the BET specific surface area is significantly enhanced upon foaming of the ASDs. For example, in the case of HP-grade-based formulations, there is a 2-5 fold increase in BET surface area of highP foams compared to control samples.

One of the most important aspects of this foaming strategy is to enhance the compaction and tabletability of the HPMCAS-based amorphous solid dispersions. For this purpose, the tabletability of milled extrudates (40% API) were studied by measuring the tablet tensile strength as a function of tableting pressure in the range of 2000-5000 psi as shown in Fig. 8a. It is evident from the compaction data that creating the cellular foam structure within the material significantly improves the tabletability and compaction properties of the amorphous solid dispersion. This is evident as the tensile strength of the tablet considerably increases at each compaction pressure. For example, the tablet tensile strength of the control 40% Std-grade samples at compaction pressures of the 2000 and 5000 psi increases from 0.49 and 0.69 MPa to 1.36 and 1.80 in lowP foam and 1.89 and 2.54 MPa in highP foam respectively.

In order to better understand the role of the foaming process on the tabletability of the extrudates, the bonding area and bonding strength [41,42] of the compacts during the tableting process should be considered. First of all, based on the specific BET surface area values (Table 2), the surface area of the foamed samples were higher than those of the control extrudates. This clearly results in much higher available surface area for the milled particles to form bonds during the compaction process. In addition, the surface morphology of the milled control and foamed extrudates of both Std- and HP-grades (Fig. 8b-d) shows that the foam samples had

Table 2
Mechanical Properties, BET Specific Surface Area and Porosity of Control and Foamed Extrudates.

Sample	Fracture Strength (MPa)	Work of Fracture (MJ/m^3)	BET Surface Area (m^2/g)	Porosity (%)
0% Std-cont	21.16 ± 0.72	417.1 ± 7.1	0.084 ± 0.002	9.9
0% Std-lowP	1.98 ± 0.09	31.9 ± 2.2	0.251 ± 0.008	50.1
0% Std-highP	1.75 ± 0.08	21.7 ± 2.6	0.277 ± 0.003	58.1
0% HP-cont	18.62 ± 0.42	359.8 ± 9.8	0.162 ± 0.002	10.5
0% HP-lowP	1.77 ± 0.27	21.4 ± 1.6	0.552 ± 0.012	53.1
0% HP-highP	1.41 ± 0.04	18.6 ± 0.9	0.614 ± 0.022	65.1
20% HP-cont	9.66 ± 0.99	113.0 ± 8.6	0.162 ± 0.002	10.1
20% HP-lowP	0.62 ± 0.02	2.4 ± 0.2	0.410 ± 0.008	34.4
20% HP-highP	0.44 ± 0.04	1.6 ± 0.1	0.439 ± 0.016	39.5
40% Std-cont	14.70 ± 1.36	100.3 ± 11.5	0.104 ± 0.007	-
40% Std-lowP	0.72 ± 0.07	2.5 ± 0.1	0.249 ± 0.011	40.1
40% Std-highP	0.28 ± 0.03	0.96 ± 0.1	0.259 ± 0.009	46.6
40% HP-cont	10.95 ± 0.73	71.2 ± 9.6	0.168 ± 0.013	-
40% HP-lowP	0.11 ± 0.01	0.2 ± 0.04	0.331 ± 0.009	32.6

Porosity for control samples with 40% drug loading was not measured because controls samples at lower drug loadings did not show much difference.

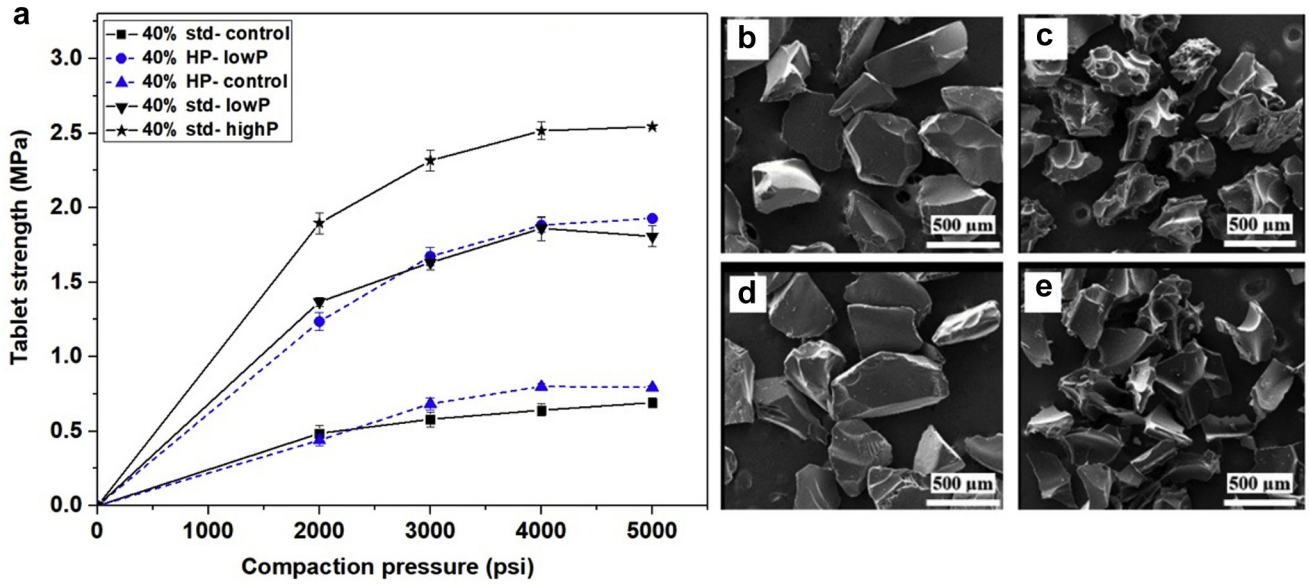

Fig. 8. (a) Tablet tensile strength as a function of compaction pressure and SEM image of milled (b) 40% HP-grade control, (c) 40% HP-grade low P, (d) 40% Std-grade control and (e) 40% Std-grade lowP extrudates.

significantly higher surface roughness and irregularities due to the break-down of the cellular structure during the milling process. This results in considerable improvement of mechanical "interlocking" of discreet particles during compaction resulting in enhancement of the bonding strength. In contrast, the milled particles of the control samples show relatively smooth surface that provide less bonding area and further difficulties during the compaction phase to form inter-particle bonds. In addition, the residual internal voids within the milled extrudates of the foam samples, ensures enhanced compressibility (reduction of volume under pressure) due to the collapse of the cell walls resulting in tablets with less internal tablet porosity.

In addition, looking closer at the specific surface are data in Table 2 and the compaction data in Fig. 8a, there are variations in correlation between the specific surface area of the extrudates and their compactibility. This is specifically true regarding the differences in specific surface area of the 40% HP-lowP sample compared to those of Std-grade. It is imperative to note that the specific area is only one factor that contributes in compactiblity of the samples. The intrinsic mechanical property of the polymer itself, plays a key role as well. The Std-grade HPMCAS has superior mechanical property (modulus, tensile strength and hardness) compared to the HP-grade due to its higher molecular weight; therefore, despite having lower porosity (surface area), the Std-grade sample forms stronger compacts.

Dissolution Studies

The results of the non-sink dissolution experiments are shown in Fig. 9. It is evident from these data that foaming the HPMCAS/ITZ amorphous solid dispersions significantly improves the dissolution rate, increases the supersaturation solubility (spring effect) as well as maintaining the supersaturation for longer periods (parachute effect) as compared to the control (unfoamed) ASDs.[43] First of all, it should be noted that hot melt extrusion of itraconazole with HPMCAS considerably improves the dissolution characteristics of the API when compared to the crystalline ITZ. This is primarily due to the amorphous nature of the API dissolved in the HPMCAS matrix with a higher energy state and lower energy barrier for solvation. In addition, the prolonged supersaturation effect is due to reduced chemical potential of the ITZ for recrystallization as well as the interactions between the HPMCAS and ITZ primarily through hydrogen bonding between the HPMCAS carboxyl groups and the carbonyl and tertiary aromatic amines of the ITZ molecule which prolongs the induction time before recrystallization of the API could take place.

As discussed before, the higher specific surface area of the foamed samples, creates a larger interface for uptake of the dissolution medium and subsequent interfacial erosion of the polymer resulting in both faster and greater dissolution of ASDs. For example, in the case of the 20% HP-grade sample, the supersaturation increases from the average of 18 µg/ml in the control sample to 47 µg/ml in the highP foam sample showing a 2.6-fold increase.

Comparing the effect of the API loading on the dissolution shows that the effect of foaming on enhancement of the dissolution characteristics of the sample is more prominent in sample with lower API content. This is evident in the dissolution properties of the ASDs containing the 20% and 40% API. It has been shown that [44] at low drug loadings, the dissolution of amorphous API is mainly governed by the dissolution of the polymer. Once the interfacial area of the polymer at polymer-water interface is eroded, the API and the polymer dissolve in the dissolution media. However, as the API content is increased, there will be a drug-rich layer after erosion of the polymer-water interfacial layer. This drug-rich layer will somewhat limit the further dissolution of the API within the medium and slows down the dissolution process.

In addition to the effect of drug loading, the grade of the HPMCAS polymer plays a key role in dissolution properties of the ASDs. Comparison of the dissolution profiles of 40% API samples in Fig. 9b and c clearly show that the HP-grade HPMCAS has a higher dissolution rate both with the control and foamed samples at similar compositions and processing conditions. This is due to the faster rate of dissolution of the low molecular weight HP-grade itself as compared to the high molecular weight Std-grade. The supersaturation kinetic profile of the HP-grade matrix is in fact governed by a dissolution-controlled mechanism with the characteristic "spring-and-parachute" release behavior. This is due to the rapid dissolution and dispersion of the HP-grade matrix in the form a colloidal moieties (as shown in Fig. 9d showing the formation of a milky dissolution media) while the Std-grade material deposited in

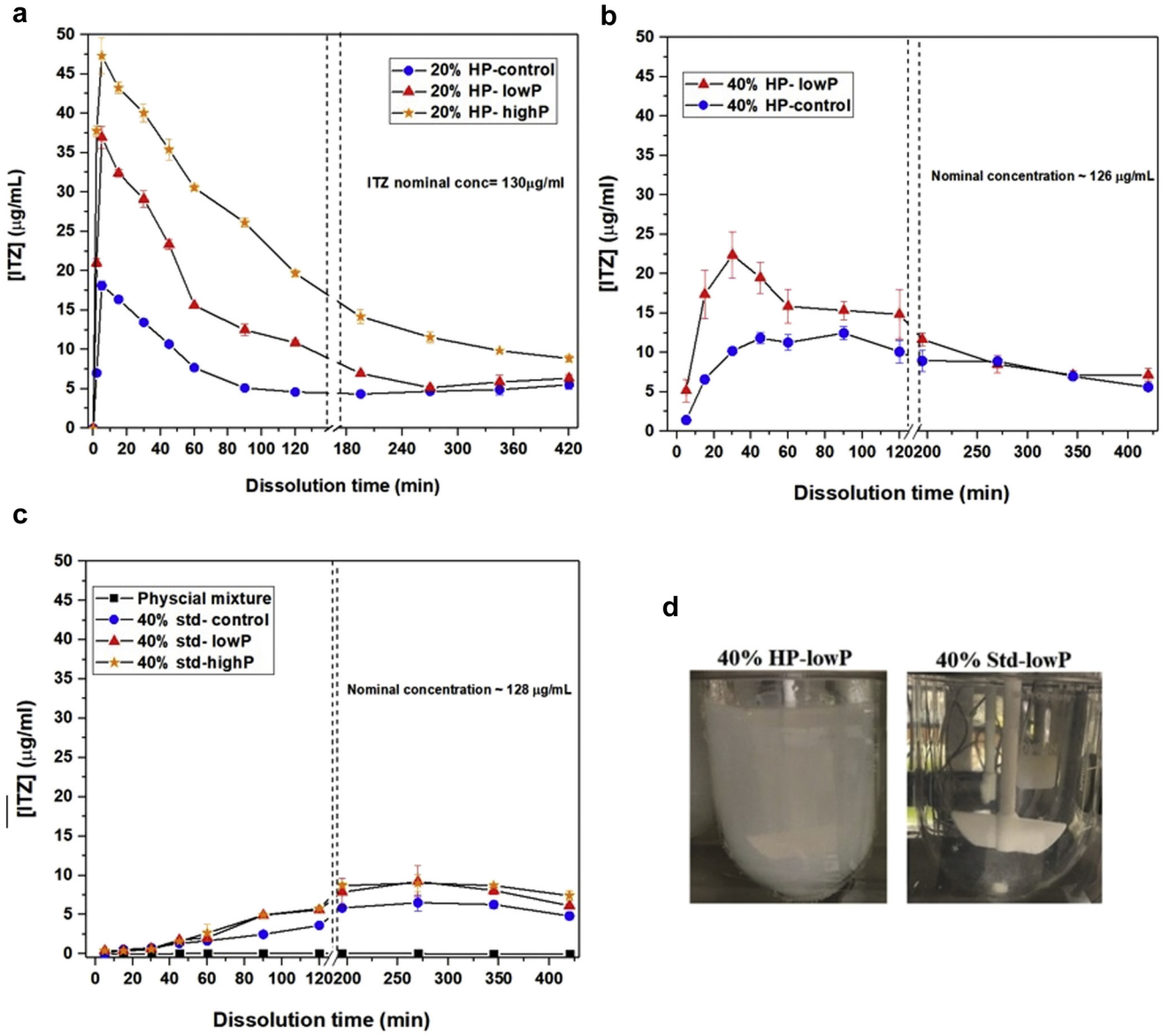

Fig. 9. Non-sink dissolution profiles of milled control and foamed extrudates in pH 6.8 phosphate buffer media using USP apparatus 2. (a) 20% HP-grade, (b) 40% HP-grade, (c) 40% Std-grade, and (d) dissolution media at 30 minutes for 40% HP- and Std-grade foamed at low pressure (tests are conducted on particle size range of 250-425 μm).

the bottom of the vessel. In contrast, the high molecular weight Std-grade material follows a more gradual release kinetic representative of a "diffusion-controlled" mechanism of the API with a considerably smaller "spring" supersaturation eventually reaching the equilibrium solubility of ITZ.[3]

Consequently, based on the dissolution profiles of the foamed samples of both grades, we can argue that creation of the foamed material with cellular morphology and increased surface area (available for erosion when in contact with the dissolution medium) can only be utilized as an efficient strategy when the carrier matrix follows a dissolution-controlled release profile. On other hand, in the case of a matrix with lower solubility that follows a diffusion-controlled release profile, foaming is found to have negligible effect on improvement of the dissolution kinetics and supersaturation due to the fact that extra interfacial area would not have a considerable effect of the underlying mechanism of the API release which is diffusion through the polymer matrix.

Conclusions

In conclusion, this study showed that the SC-CO_2 foam extrusion process for preparation of amorphous solid dispersions of HPMCAS and itraconazole with two grades of high molecular weight (Std-grade) and low molecular weight (HP-grade) polymers can be successfully applied without affecting the crystallinity of the API within the polymer matrix. It was shown that foaming of these ASDs result in improvement of milling efficiency and tabletability due to formation of porous and smaller particles during the milling process. In addition, the rheological properties of the ASDs showed that the Std-grade sample had higher viscosity and melt strength that is necessary for achieving a stable cellular structure especially as the API content increases. In contrast, the HP-grade polymer with lower viscosity showed significant dependency of the viscoelastic properties on the API content and subsequent compromise of the cellular structure at high API content due to insufficient melt

strength. The dissolution profiles of the foams showed that foaming can be considerably effective in improving the supersaturation concentration and maintaining a prolonged supersaturation in the case of HP-grade while only minimal improvement observed in the case of Std-grade. This was attributed to the different mechanisms of dissolution of these amorphous solid dispersions. Overall, this study showed that the HP-grade HPMCAS polymer is a suitable candidate for preparation of amorphous solid dispersion with robust milling property, higher compatibility with the foaming process, ease of processing and fast "dissolution-erosion" controlled release profile.

Acknowledgement

Kind assistance of Mr. Glen S Baum with the porosity measurements is gratefully acknowledged.

This work was financially supported by PhRMA foundation.

Appendix A. Supplementary Data

Supplementary data to this article can be found online at https://doi.org/10.1016/j.xphs.2020.11.038

References

1. Duarte Í, Santos JL, Pinto JF, Temtem M. Screening Methodologies for the Development of Spray-Dried Amorphous Solid Dispersions. *Pharm Res*. 2015;32(1):222-237.
2. Jermain SV, Brough C, Williams RO. Amorphous solid dispersions and nanocrystal technologies for poorly water-soluble drug delivery – An update. *Int J Pharm*. 2018;535(1):379-392.
3. Sun DD, Lee PI. Haste Makes Waste: The Interplay Between Dissolution and Precipitation of Supersaturating Formulations. *AAPS J*. 2015;17(6):1317-1326.
4. Baghel S, Cathcart H, O'Reilly NJ. Polymeric amorphous solid dispersions: a review of amorphization, crystallization, stabilization, solid-state characterization, and aqueous solubilization of biopharmaceutical classification system class ii drugs. *J. Pharm Sci*. 2016;105(9):2527-2544.
5. Brouwers J, Brewster ME, Augustijns P. Supersaturating Drug Delivery Systems: The Answer to Solubility-Limited Oral Bioavailability? *J Pharm Sci*. 2009;98(8):2549-2572.
6. Warren DB, Benameur H, Porter CJH, Pouton CW. Using polymeric precipitation inhibitors to improve the absorption of poorly water-soluble drugs: A mechanistic basis for utility. *J Drug Target*. 2010;18(10):704-731.
7. Sarode AL, Sandhu H, Shah N, Malick W, Zia H. Hot melt extrusion (HME) for amorphous solid dispersions: predictive tools for processing and impact of drug–polymer interactions on supersaturation. *Eur J Pharm Sci*. 2013;48(3):371-384.
8. Crowley MM, Zhang F, Repka MA, Thumma S, Upadhye SB, Kumar Battu S, McGinity JW, Martin C. Pharmaceutical applications of hot-melt extrusion: part I. *Drug Dev Ind Pharm*. 2007;33(9):909-926.
9. Repka MA, Battu SK, Upadhye SB, Thumma S, Crowley MM, Zhang F, Martin C, McGinity JW. Pharmaceutical applications of hot-melt extrusion: Part II. *Drug Dev Ind Pharm*. 2007;33(10):1043-1057.
10. Patil H, Tiwari RV, Repka MA. Hot-melt extrusion: from theory to application in pharmaceutical formulation. *AAPS PharmSciTech*. 2016;17(1):20-42.
11. Leuner C, Dressman J. Improving drug solubility for oral delivery using solid dispersions. *Eur J Pharm Biopharm*. 2000;50(1):47-60.
12. Serajuddin AT. Solid dispersion of poorly water-soluble drugs: Early promises, subsequent problems, and recent breakthroughs. *J Pharm Sci*. 1999;88(10):1058-1066.
13. Schenck L, Lowinger M, Troup GM, Li L, McKelvey C. Achieving a hot melt extrusion design space for the production of solid solutions. *Chem Eng Pharm Ind Drug Product Design Dev Model*. 2019:469-487.
14. Li Y, Pang H, Guo Z, Lin L, Dong Y, Li G, Lu M, Wu C. Interactions between drugs and polymers influencing hot melt extrusion. *J Pharm Pharmacol*. 2014;66(2):148-166.
15. Repka MA, Majumdar S, Kumar Battu S, Srirangam R, Upadhye SB. Applications of hot-melt extrusion for drug delivery. *Expert Opin Drug Del*. 2008;5(12):1357-1376.
16. Lang B, McGinity JW, Williams III RO. Hot-melt extrusion–basic principles and pharmaceutical applications. *Drug Dev Ind Pharm*. 2014;40(9):1133-1155.
17. Repka MA, Koleng JJ, Zhang F, McGinity JW. Encyclopedia of Pharmaceutical Science and Technology. 4th ed. Swarbrick J., editor. Boca Raton: Taylor & Francis; 2013. Hot-melt Extrusion Technology; p.22. 4296p.
18. Friesen DT, Shanker R, Crew M, Smithey DT, Curatolo WJ, Nightingale JAS. Hydroxypropyl Methylcellulose Acetate Succinate-Based Spray-Dried Dispersions: An Overview. *Mol Pharm*. 2008;5(6):1003-1019.
19. Ting JM, Navale TS, Jones SD, Bates FS, Reineke TM. Deconstructing HPMCAS: excipient design to tailor polymer–drug interactions for oral drug delivery. *ACS Biomater Sci Eng*. 2015;1(10):978-990.
20. Obara S, Tanno FK, Sarode A. Chapter 4: Properties and Applications of Hypromellose Acetate Succinate (HPMCAS) for Solubility Enhancement Using Melt Extrusion. In: Repka MA, Langley N, DiNunzio J, eds. *Melt Extrusion: Materials, Technology and Drug Product Design*. New York: Springer; 2013:107-121.
21. Heck III RL. A review of commercially used chemical foaming agents for thermoplastic foams. *J Vinyl Addit Techn*. 1998;4(2):113-116.
22. Mohebbi A, Mighri F, Ajji A, Rodrigue D. Current issues and challenges in polypropylene foaming: a review. *Cell Polym*. 2015;34(6):299-338.
23. Okolieocha C, Raps D, Subramaniam K, Altstädt V. Microcellular to nanocellular polymer foams: Progress (2004–2015) and future directions–A review. *Eur Polym J*. 2015;73:500-519.
24. Colton J, Suh N. The nucleation of microcellular thermoplastic foam with additives: Part I: Theoretical considerations. *Polym Eng Sci*. 1987;27(7):485-492.
25. Verreck G, Decorte A, Li H, Tomasko D, Arien A, Peeters J, Rombaut P, Van den Mooter G, Brewster ME. The effect of pressurized carbon dioxide as a plasticizer and foaming agent on the hot melt extrusion process and extrudate properties of pharmaceutical polymers. *J. Supercrit. Fluids*. 2006;38(3):383-391.
26. Verreck G, Decorte A, Heymans K, Adriaensen J, Cleeren D, Jacobs A, Liu D, Tomasko D, Arien A, Peeters J. The effect of pressurized carbon dioxide as a temporary plasticizer and foaming agent on the hot stage extrusion process and extrudate properties of solid dispersions of itraconazole with PVP-VA 64. *Eur J Pharm Sci*. 2005;26(3-4):349-358.
27. Ashour A, Kulkarni EV, Almutairy B, Park J-B, Shah SP, Majumdar S, Lian Z, Pinto E, Bi V, Durig T. Influence of pressurized carbon dioxide on ketoprofen-incorporated hot-melt extruded low molecular weight hydroxypropylcellulose. *Drug Dev Ind Pharm*. 2016;42(1):123-130.
28. Vo AQ, Feng X, Zhang J, Zhang F, Repka MA. Dual mechanism of microenvironmental pH modulation and foam melt extrusion to enhance performance of HPMCAS based amorphous solid dispersion. *Int J Pharm*. 2018;550(1-2):216-228.
29. Tye CK, Sun C, Amidon GE. Evaluation of the effects of tableting speed on the relationships between compaction pressure, tablet tensile strength, and tablet solid fraction. *J Pharm Sci*. 2005;94(3):465-472.
30. Almutairi M, Almutairy B, Sarabu S, Almotairy A, Ashour E, Bandari S, Batra A, Tewari D, Durig T, Repka MA. Processability of AquaSolve™ LG polymer by hot-melt extrusion: effects of pressurized CO2 on physicomechanical properties and API stability. *J Drug Deliv Sci Tec*. 2019;52:165-176.
31. Shin HY, Wu J. Equation of State for the Phase Behavior of Carbon Dioxide–Polymer Systems. *Ind Eng Chem*. 2010;49(16):7678-7684.
32. Bray CL, Tan B, Higgins S, Cooper AI. Polymer CO2 Solubility. Structure/Property Relationships in Polyester Libraries. *Macromolecules*. 2010;43(22):9426-9433.
33. Spitael P, Macosko CW. Strain hardening in polypropylenes and its role in extrusion foaming. *Polym Eng Sci*. 2004;44(11):2090-2100.
34. Xu Z, Zhang Z, Guan Y, Wei D, Zheng A. Investigation of extensional rheological behaviors of polypropylene for foaming. *J Cell Plast*. 2013;49(4):317-334.
35. Ramesh N, Lee S. Blowing agent effect on extensional viscosity calculated from fiber spinning method for foam processing. *J Cell Plast*. 2000;36(5):374-385.
36. Nam G, Yoo J, Lee J. Effect of long-chain branches of polypropylene on rheological properties and foam-extrusion performances. *J Appl Polym Sci*. 2005;96(5):1793-1800.
37. Stange J, Münstedt H. Effect of long-chain branching on the foaming of polypropylene with azodicarbonamide. *J Cell Plast*. 2006;42(6):445-467.
38. Rizvi A, Tabatabaei A, Barzegari MR, Mahmood SH, Park CB. In situ fibrillation of CO2-philic polymers: Sustainable route to polymer foams in a continuous process. *Polym*. 2013;54(17):4645-4652.
39. Barnes H, Roberts G. A simple empirical model describing the steady-state shear and extensional viscosities of polymer melts. *J Non-Newton Fluid*. 1992;44:113-126.
40. Laguna-Gutierrez E, Van Hooghten R, Moldenaers P, Rodriguez-Perez MA. Understanding the foamability and mechanical properties of foamed polypropylene blends by using extensional rheology. *J Appl Polym Sci*. 2015;132(33).
41. Osei-Yeboah F, Chang S-Y, Sun CC. A critical examination of the phenomenon of bonding area-bonding strength interplay in powder tableting. *Pharm Res*. 2016;33(5):1126-1132.
42. Nyström C, Alderborn G, Duberg M, Karehill P-G. Bonding surface area and bonding mechanism-two important factors fir the understanding of powder comparability. *Drug Dev Ind Pharm*. 1993;19(17-18):2143-2196.
43. Liu C, Chen Z, Chen Y, Lu J, Li Y, Wang S, Wu G, Qian F. Improving oral bioavailability of sorafenib by optimizing the "spring" and "parachute" based on molecular interaction mechanisms. *Mol Pharm*. 2016;13(2):599-608.
44. Alonzo DE, Gao Y, Zhou D, Mo H, Zhang GG, Taylor LS. Dissolution and precipitation behavior of amorphous solid dispersions. *J Pharm Sci*. 2011;100(8):3316-3331.